Exploration of Foods and Foodomics

Open Exploration

Open Access Original Article

Green synthesis and characterization of La-doped ZnO nanoparticles using pineapple peel extract: a sustainable approach to improve functional properties

Rabia Tasaduq Hussain[1], Nadheera Alwanee Pandi[1], Hamidah Abdullah[1], Jun Haslinda Shariffuddin[1,2*]

[1]Faculty of Chemical and Process Engineering Technology, Universiti Malaysia Pahang Al-Sultan Abdullah, Kuantan 26300, Malaysia

[2]Centre for Sustainability of Mineral and Resource Recovery Technology (Pusat SMaRRT), Universiti Malaysia Pahang Al-Sultan Abdullah, Kuantan 26300, Malaysia

***Correspondence:** Jun Haslinda Shariffuddin, Faculty of Chemical and Process Engineering Technology, Universiti Malaysia Pahang Al-Sultan Abdullah, Lebuhraya Persiaran Tun Khalil Yaakob, Kuantan 26300, Malaysia; Centre for Sustainability of Mineral and Resource Recovery Technology (Pusat SMaRRT), Universiti Malaysia Pahang Al-Sultan Abdullah, Lebuhraya Persiaran Tun Khalil Yaakob, Kuantan 26300, Malaysia. junhaslinda@umpsa.edu.my

Academic Editor: Sandra R. S. Ferreira, Federal University of Santa Catarina, Brazil

Received: September 3, 2025 **Accepted:** March 20, 2026 **Published:** April 29, 2026

Cite this article: Hussain RT, Pandi NA, Abdullah H, Shariffuddin JH. Green synthesis and characterization of La-doped ZnO nanoparticles using pineapple peel extract: a sustainable approach to improve functional properties. Explor Foods Foodomics. 2026;4:1010141. https://doi.org/10.37349/eff.2026.1010141

Abstract

Aim: The aim of this study is to synthesize and characterize the more efficient photocatalyst [zinc oxide nanoparticles (ZnONPs)] via the addition of dopant lanthanum (La) and pineapple peel extract. Pineapple peel as a green source consists of bioactive compounds that work as a capping agent and reducer for our La-doped ZnONPs (La-ZnONPs) and shield against the aggregation of nanoparticles. In addition, this study evaluates the influence of La doping on their structural and optical properties for photocatalytic applications.

Methods: La-ZnONPs were modified and fabricated efficiently with the simple co-precipitation method with pineapple extract in this research work. The materials (La-ZnONPs) were thoroughly characterized by various spectroscopic techniques like X-ray diffraction (XRD), fourier transform infrared spectroscopy (FTIR), scanning electron microscopy-energy dispersive X-ray (SEM-EDX), ultra-violet visible (UV-Vis) spectroscopy and Brunauer-Emmett-Teller (BET) analysis.

Results: This study effectively demonstrates the effect of concentration of La dopant on the La-ZnONPs fabrication such as elevation of La concentration from 1% to 3% in ZnO results in an augmentation of crystallite size (from 27.25 to 21.27 nm), accompanied by a corresponding shift in bandgap values (3.21 to 3.11 eV) along with surface area, and induces a morphological transformation after treatment.

Conclusions: It was concluded that combining La doping with a green synthesis route provides an environmentally sustainable pathway for producing ZnO-based nanomaterials with improved functional properties.

Keywords

co-precipitation, La-doped ZnONPs, pineapple, ZnONPs, zinc acetate dihydrate, bioactive compounds

Introduction

Zinc oxide nanoparticles (ZnONPs) in nanotechnology have dominated nanomaterials as an area of interest for researchers due to their wide bandgap, high exciton binding energy, given their importance in diverse applications, including electronics, biomedical engineering, and photocatalysis [1–4]. Improving the functional properties of ZnONPs often relies on modifying their structure through the infusion of rare-earth elements. Among which lanthanum (La^{3+}) doping is an ideal candidate to change the electronic states, lower the bandgap energy, and enhance the surface reactivity. Recent studies indicated that La-doped ZnONPs (La-ZnONPs) exhibit better crystallinity, increased defect density, and improved light-harvesting properties [5–8]. These properties make them promising candidates for photocatalytic and semiconductor applications.

Concurrently, green synthesis is considered as sustainable replacement for conventional chemical routes, which rely on toxic chemicals, high temperatures, or energy-intensive processes. Plant extracts are most appealing because they are rich in bioactive compounds such as polyphenols, flavonoids, and organic acids that act as reducing, capping, and stabilizing agents [9–12]. This phytochemical-mediated approach helps to avoid hazardous chemicals and supports the circular economy by using waste valorization principles. Numerous biological sources such as aloe vera, banana peel, and citrus extracts have been used to modify metal oxide nanoparticles; however, their efficiency depends on specific phytochemical composition and reducing ability [13, 14].

Pineapple peel extract (PPE) is abundant in phytochemical compounds, which are particularly valuable for extracting bioactive functional groups that enable strong chelation between metal ions and efficient nanoparticle stabilization. These phytochemicals serve as capping agents, preventing nanoparticle agglomeration and enhancing their stability [11, 15, 16]. Exploring sustainable ways to utilize pineapple waste, such as peels, crown, stem, in diverse ways not only reduces its negative environmental footprint but also unlocks its potential in diverse applications. One innovative method involves utilizing this biodegradable biomass as a precursor for synthesizing nanoparticles through eco-friendly processes [2, 17, 18]. Despite containing a high phytochemical content and being easily available as an agricultural waste globally, its potential remains underexplored for the green synthesis of La-ZnONPs. Many studies focus on undoped ZnONPs, but there is no published work that addresses the incorporation of La^{3+} into ZnONPs using PPE as a green reducing and capping agent. Current work on La-ZnONPs almost exclusively uses chemical precipitation or high-temperature calcination methods that lack an environmentally friendly green synthesis route.

We hypothesize that a higher concentration of La dopant into ZnONPs will systematically modulate its key physicochemical properties, such as crystallite size, bandgap energy, morphology, and surface area. It is done due to two factors, such as lattice distortion and surface modification induced by La^{3+} incorporation and interactions with the phytochemicals present in PPE [5, 19]. This study aims to fabricate La-ZnONPs using PPE as a phytochemical reducing agent by varying the La dopant concentrations. By integrating rare-earth doping with a green synthesis approach, this work introduces a sustainable pathway for producing modified ZnO nanomaterials and provides new insight into dopant-induced property evolution under phytochemical-assisted synthesis conditions. To the best of our knowledge, many researchers utilize La as dopant to increase the efficiency of nanoparticles, but along with green sources such as pineapple extract, as in this study, is a novel aspect added to the field of nanotechnology to increase the efficiency and potential of photocatalysts in future.

Materials and methods

Raw materials and reagents

Pineapple peels were sourced from a local market in Gambang, Malaysia. Zinc acetate dihydrate [$Zn(CH_3COO)_2 \cdot 2H_2O$, ≥ 99%; Cat. No. 379749], sodium hydroxide (NaOH, ≥ 97%; Cat. No. S8045), and La nitrate hexahydrate [$La(NO_3)_3 \cdot 6H_2O$, 99.9%; Cat. No. 449830] were of analytical grade and obtained from Sigma-Aldrich (Malaysia). Distilled and deionized water were supplied by the UMPSA laboratory for the experiments.

Preparation of aqueous PPE

The peels of pineapple were thoroughly washed with distilled water to eliminate dirt. The peels were dried in an oven (MEMMERT UF11, Germany) at 60°C for 4 h and grounded it in coarse powder with the help of a heavy-duty grinder (SHANICE 1600W, China). This temperature is commonly used in green synthesis to remove moisture while preserving polyphenols and sugars essential for reduction and capping [20, 21]. For each batch, 10 g of grounded product was boiled in 100 mL of deionized water in a beaker at 70°C to 80°C for half an hour, producing a PPE. The solution was filtered through filter paper, yielding a brownish-yellow filtrate. This filtrate can be saved at 4°C in a chiller (MEMMERT IPP500, Germany) for further use.

Fabrication of ZnONPs and La-ZnONPs

A straightforward co-precipitation procedure outlined in reference [5, 10] was used to fabricate ZnONPs. Ten milliliters of distilled water and 50 mL of PPE were mixed in a 500 mL beaker with 4 g of $Zn(CH_3COO)_2 \cdot 2H_2O$ in this mixture at constant stirring. The pH of the solution was gradually raised to 11–12 by adding 0.1 M NaOH. The white precipitation of $Zn(OH)_2$ is shown at the moment of the addition of NaOH. The solution was stirred continuously for 1 h at 40°C to 50°C and then centrifuged for 1 min at 1,800 *g* once it had cooled to room temperature. After 6 h of drying at 120°C, a white precipitate was formed from the resultant material, which was subsequently crushed into a fine powder using a mortar and pestle (Chembio, Malaysia) and followed by calcination at 300°C. The undoped ZnONPs were collected accordingly.

For La doping, $La(NO_3)_3 \cdot 6H_2O$ was introduced at a concentration of 1%, 2%, and 3% by weight during the precipitation step. Each suspension was stirred for 1 h at 45–50°C. After 1 h reaction, each suspension was centrifuged for 1 min at 1,800 *g*. This is sufficient because the intermediate $Zn(OH)_2$ precipitate forms an aggregate before calcination. The precipitate was washed three times with DI water and twice with ethanol to remove residual NaOH and hydroxide ions. It was repeated before with undoped ZnONPs also. Then, after drying at 120°C for 6 h performed to achieve a white precipitate as the resultant material, which was subsequently crushed into a fine powder using a mortar and pestle, and followed by calcination at 300°C. This temperature helps to convert $Zn(OH)_2$ into ZnO and removes organic residues. It aligns with prior green synthesis protocols (250–400°C). Separate syntheses were performed for each La concentration. The schematic representation for fabrication is depicted in Figure 1.

Analysis of La-ZnONPs

The fabricated La-ZnONPs were analyzed using X-ray diffraction (XRD), fourier transform infrared spectroscopy (FTIR), scanning electron microscopy-energy dispersive X-ray (SEM-EDX), ultra-violet visible (UV-Vis) spectroscopy, and Brunauer-Emmett-Teller (BET) techniques. FTIR (Thermo Fisher Scientific, Nicolet iS50, USA) was employed to study the absorption patterns and identify functional groups present in fabricated materials. XRD analysis has been performed employing the PANalytical/X'Pert^3 Powder from Netherland (Malvern Panalytical) to confirm the crystalline structure of the ZnONPs. Equation 1 depicts the calculation of crystallite size (D) to analyze the effect of increasing dopant concentration on the fabrication of La-ZnONPs. The SEM-EDX analysis was performed employing the JSM-IT200 InTouchScope™ (Hitachi, Japan) to investigate the morphological characteristics and elemental composition of the resultant by-product. To prevent charging during the analysis, the powders were sputter-coated with a fine layer of gold. UV-Vis spectroscopy (Perkin Elmer, Model 50 Probe, UK) was utilized to evaluate the transmitted light

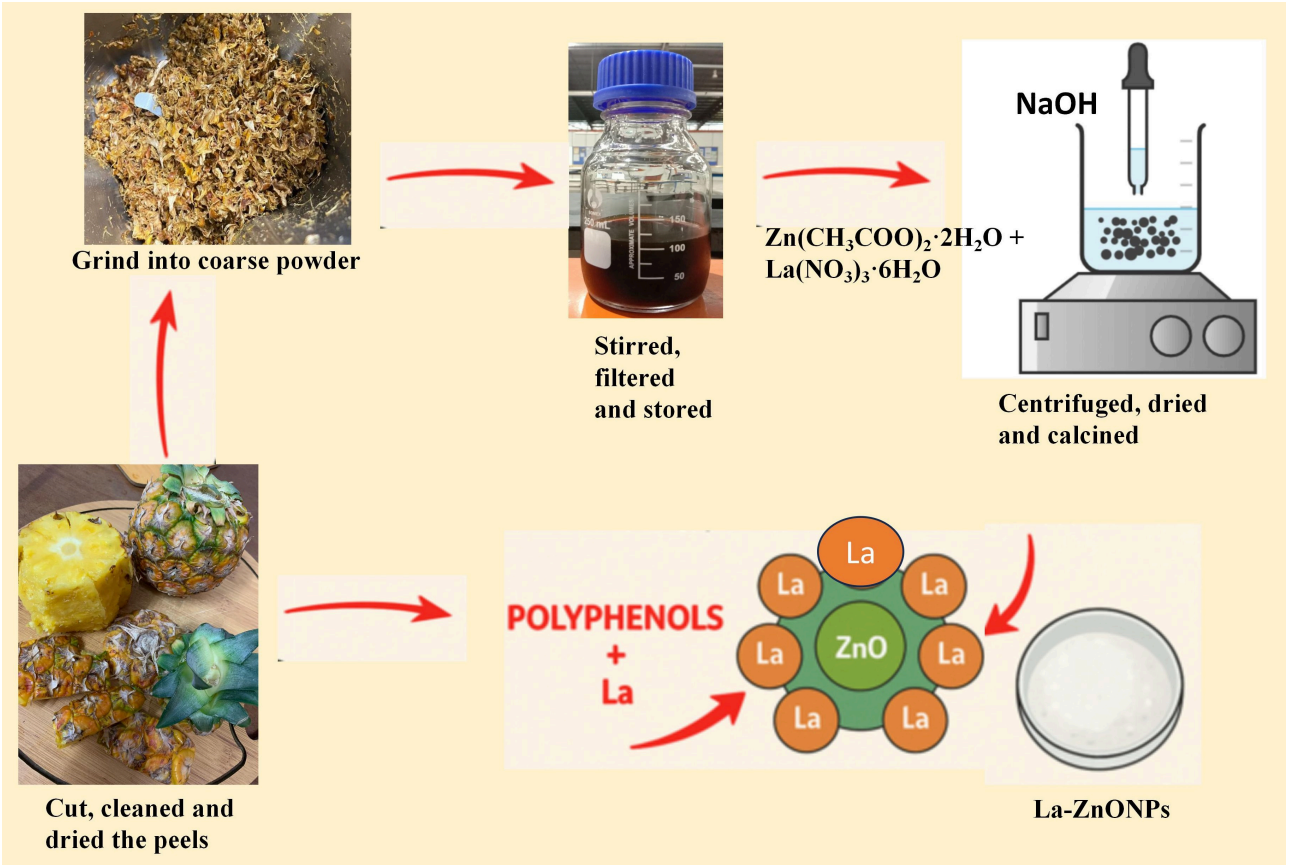

Figure 1. Representation for the fabrication of La-ZnONPs. $Zn(CH_3COO)_2 \cdot 2H_2O$: zinc acetate dihydrate; $La(NO_3)_3 \cdot 6H_2O$: lanthanum nitrate hexahydrate; NaOH: sodium hydroxide; La: lanthanum; La-ZnONPs: La-doped zinc oxide nanoparticles.

through the sample in comparison to a reference, or blank. Prior to conducting the analysis, the wavelength was calibrated to 800 nm. BET analysis has been done to obtain the specific surface area using nitrogen physisorption isotherms at liquid nitrogen temperature on a Micromerimetics version 4.02 BET instrument (ASAP2020, Germany).

$$D = \frac{0.9\lambda}{\beta cos\theta} \quad (1)$$

In the equation, D, λ, β, and θ represent the average crystal size (in nm), the wavelength, the full width at half maximum (FWHM) of the XRD peak (in radians), and the maximum angle of Bragg diffraction peak (in radians), respectively.

Results

XRD patterns ranging between 20° to 80° depicted in Figure 2A for undoped ZnONPs and 1%, 2%, and 3% La-ZnONPs reveal peaks characteristic of the hexagonal wurtzite ZnO structure (JCPDS No. 36-1451) with the highest reflections between 30° to 40° corresponding to the (001), (002), and (101) planes of ZnONPs, respectively [6, 22]. The dominant (101) peak appears at 2θ angles of 36.296, 36.307, 36.298, and 36.351 with minor variation in peak position as La concentration increases (Figure 2B).

FTIR analysis of the extract and its interaction with fabricated ZnONPs and dopant concentration at 1%, 2%, and 3% on ZnONPs at room temperature reveals distinctive bands in the range of 400 to 4,000 cm^{-1} shown in Figure 3. The pineapple extract consisted of various chemical constituents, primarily carbohydrates and phenolic compounds, with minimal quantities of flavonoids. The bioorganic compounds present hydroxyl functional groups (O–H) at 3,312 cm^{-1}, carbonyl moieties (C=O) at 1,632 cm^{-1}, aromatic linkages (C=C) at 1,389 cm^{-1}, and C–O stretching at 1,039 cm^{-1} (Figure 3a), which are vital for enhancing the biogenic generation of ZnONPs. The pineapple extract confirms the presence of carbonyl-rich biomolecules, which played a role in reducing and stabilizing the nanoparticles.

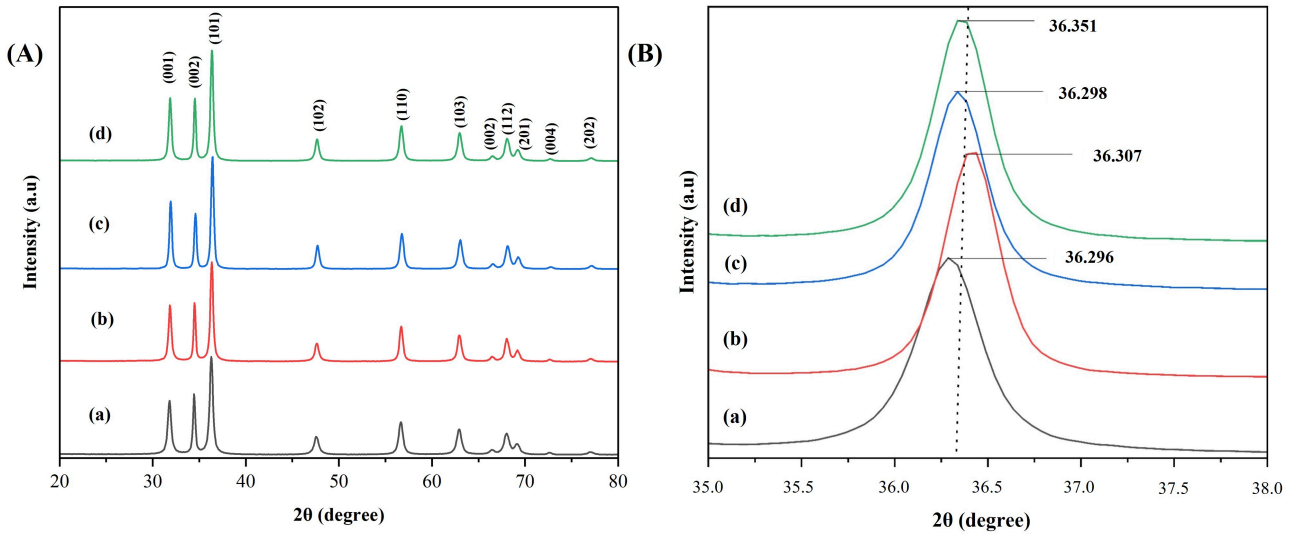

Figure 2. XRD pattern for (a) ZnONPs, (b) 1% La-ZnONPs, (c) 2% La-ZnONPs, and (d) 3% La-ZnONPs (left side, A) and XRD highest peak in zoom in to distinguish level (right side, B). Intensity is expressed in arbitrary units (a.u). XRD: X-ray diffraction; ZnONPs: zinc oxide nanoparticles; La-ZnONPs: lanthanum-doped ZnONPs.

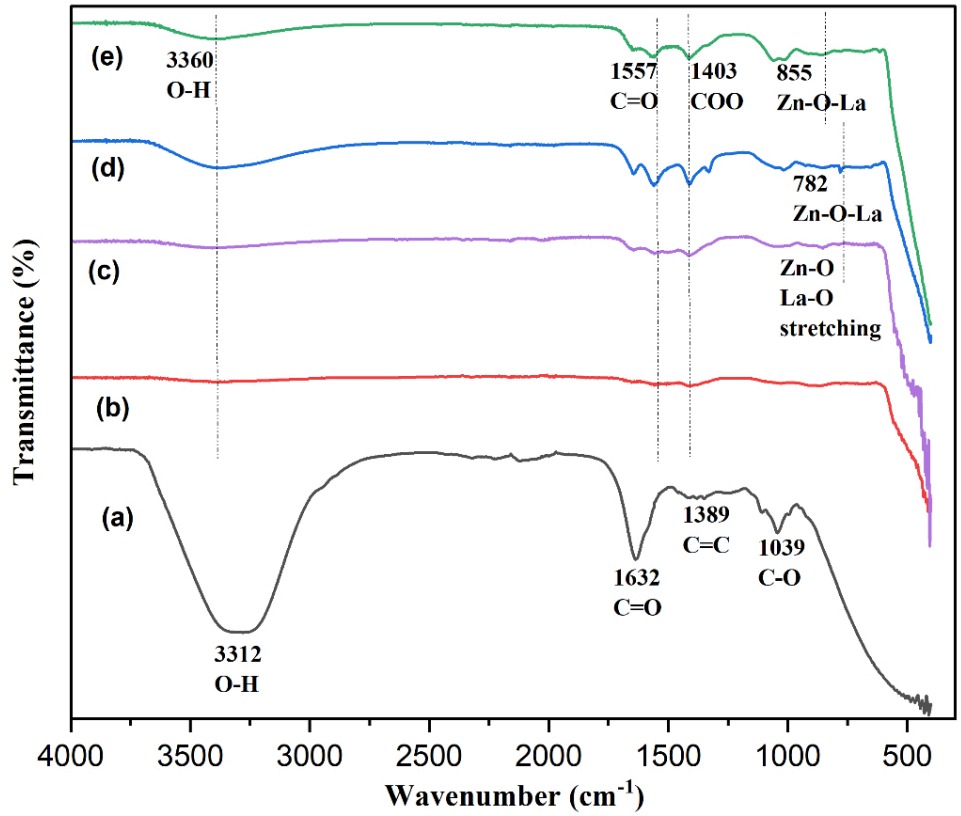

Figure 3. FTIR spectra of pineapple extract (a), ZnONPs (b), 1% La-ZnONPs (c), 2% La-ZnONPs (d), and 3% La-ZnONPs (e). La: lanthanum; FTIR: fourier transform infrared spectroscopy; ZnONPs: zinc oxide nanoparticles; La-ZnONPs: La-doped ZnONPs.

The fabricated doped and undoped ZnONPs are analyzed morphologically by SEM-EDX data. The SEM images are displayed below in Figure 4. Morphologically images showed significantly nanoflower petals' shape as the dopant concentration increased due to the increment of dopant inside the matrix of ZnONPs to provide a larger surface area. The elemental composition of Zn in the ZnONPs was analyzed through EDX to determine the elements in the sample of the powder. Figure 4 displays the EDX spectra for various synthesized ZnONPs.

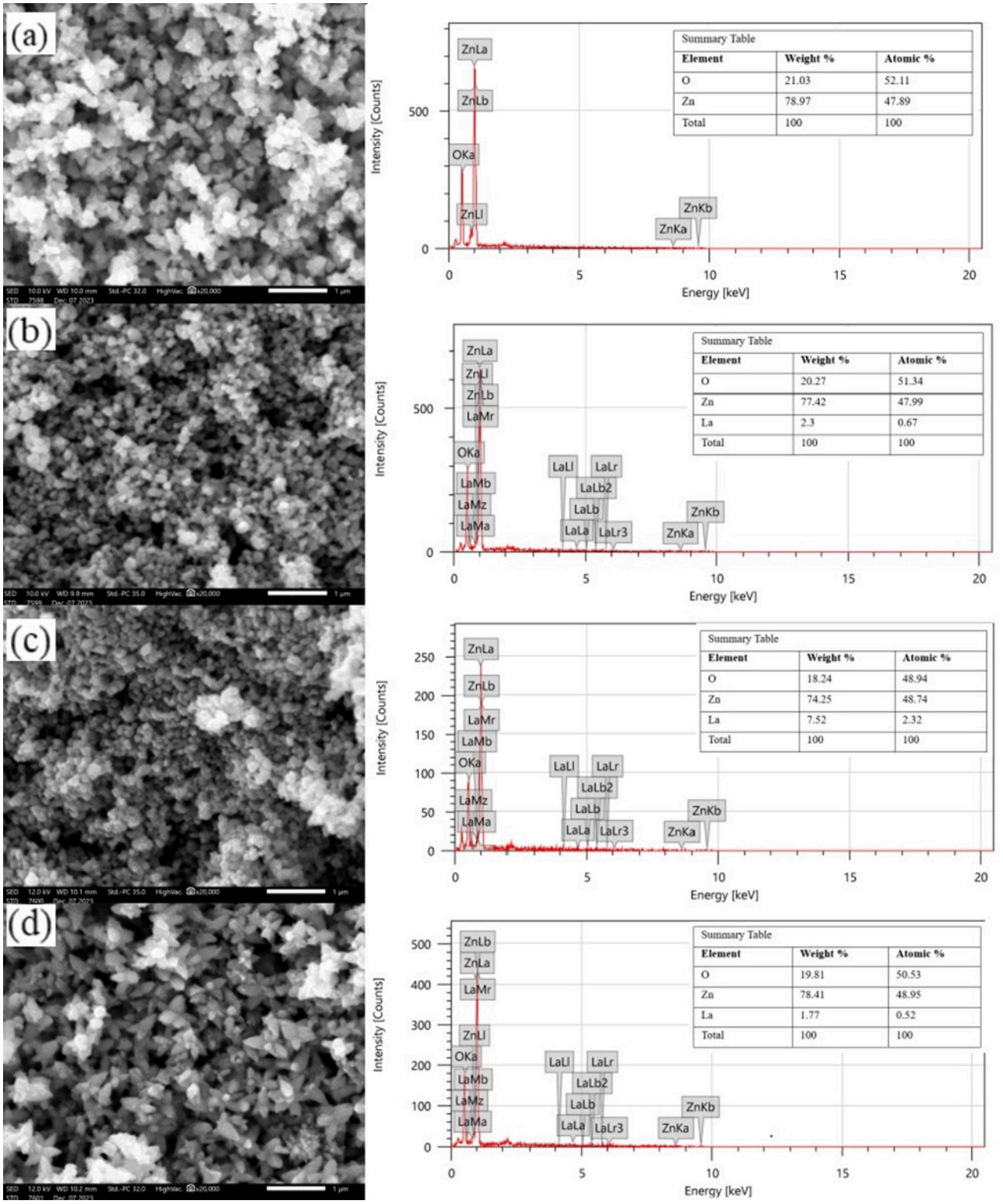

Figure 4. SEM depictions of (a) undoped ZnONPs at 300°C at 20,000× magnification, (b) 1% La-ZnONPs for 300°C at 20,000× magnification, (c) 2% La-ZnONPs at 300°C at 20,000× magnification, and (d) 3% La-ZnONPs at 300°C at 20,000× magnification, with respective EDX data besides each SEM images (scale bar = 1 μm). La: lanthanum; EDX: energy dispersive X-ray; SEM: scanning electron microscopy; ZnONPs: zinc oxide nanoparticles; La-ZnONPs: La-doped ZnONPs.

The optical properties of ZnONPs and La-ZnONPs materials with three doping concentrations were analyzed by UV-Vis absorption spectra, represented in Figure 5. The absorption spectra show that 1%, 2%, and 3% La-ZnONPs have peaks at 410 nm, 420 nm, and 429 nm, while undoped ZnONPs have peaks at 397 nm. By analyzing the variation of $(\alpha h\nu)^2$ and energy as a function of $h\nu$ (Figure 6), the calculated bandgap values were determined to be 3.21, 3.18, 3.13, and 3.11 eV for ZnONPs and La-ZnONPs with 1%, 2%, and 3% La^{3+} ions, respectively.

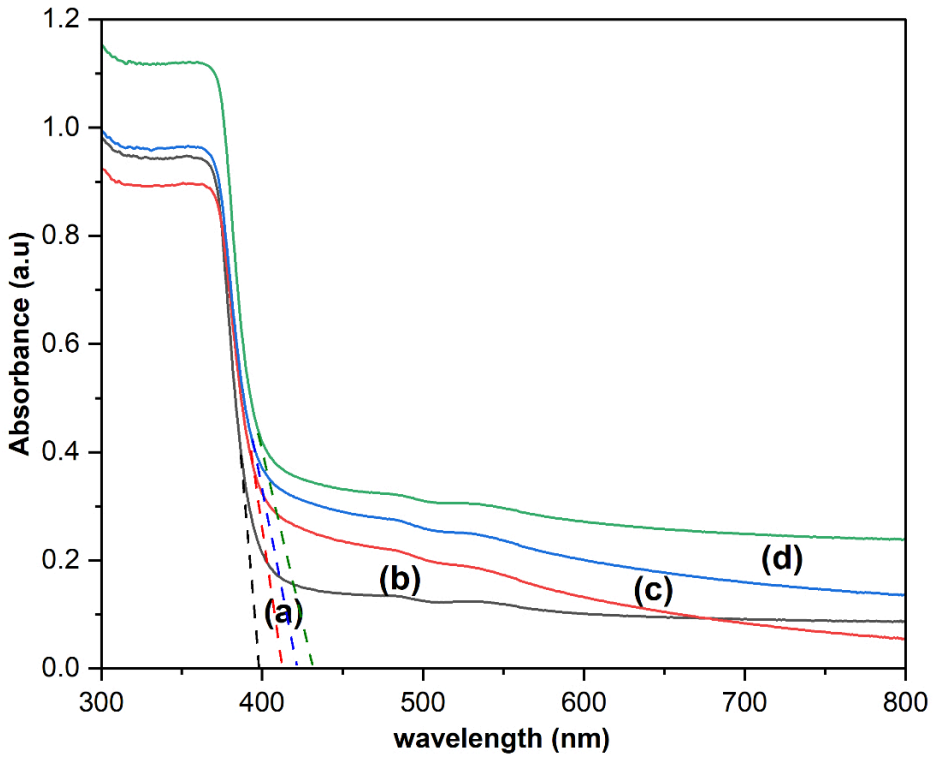

Figure 5. UV-Vis plot for (a) undoped ZnONPs, (b) 1% La-ZnONPs, (c) 2% La-ZnONPs, and (d) 3% La-ZnONPs. UV-Vis: ultra-violet visible; ZnONPs: zinc oxide nanoparticles; La-ZnONPs: lanthanum-doped ZnONPs.

The assessment of surface area utilizing the BET methodology was undertaken to elucidate the surface characteristics of undoped ZnONPs and La-ZnONPs. Upon the deposition of La-ZnONPs, the La-ZnONPs exhibited a noteworthy enhancement in specific surface area, escalating from 37.1206 to 65.4184 m^2/g. BJH pore-size distribution analyses show that undoped ZnONPs have a narrow distribution (12–18 nm), while La-doped samples exhibit broader distributions and increased pore volume.

Discussion

The combined characterization techniques demonstrate that La incorporation and the presence of PPE significantly influence the structural, morphological, optical, and surface properties of ZnONPs synthesized through green co-precipitation.

XRD results indicate a reduction in crystallite size with increasing La content. A slight broadening of the (101) peak is observed with increasing La content, which corresponds to a reduction in crystallite size, as shown in Figure 2B. To enable clearer comparison, peak parameters of the main (101) peak, including 2θ value, FWHM, and crystallite size, were summarized in Table 1. Equation 1 is used to calculate the crystallite size (D) to analyze the effect of increasing dopant concentration on the fabrication of La-ZnONPs. On the basis of calculations derived from XRD analysis, the increased dopant content decreases the crystallite size from 27.25 nm to 21.27 nm, as shown by the decreasing trend in Table 2. Although doping can sometimes cause measurable peak shifting, the variations in 2θ in this study fall within the typical range reported for low-level rare-earth doping and do not indicate a clear systematic shift.

Table 1. Peak parameters of the dominant (101) XRD reflection.

Samples	2θ (degree)	Lattice plane (hkl)	FWHM (β) (degree)	Crystallite size (nm)
ZnONPs	36.296	(101)	0.3058	28.55
1% La-ZnONPs	36.307	(101)	0.3156	27.67
2% La-ZnONPs	36.298	(101)	0.3258	26.80
3% La-ZnONPs	36.351	(101)	0.3625	24.09

XRD: X-ray diffraction; FWHM: full width at half maximum; ZnONPs: zinc oxide nanoparticles; La-ZnONPs: lanthanum-doped ZnONPs.

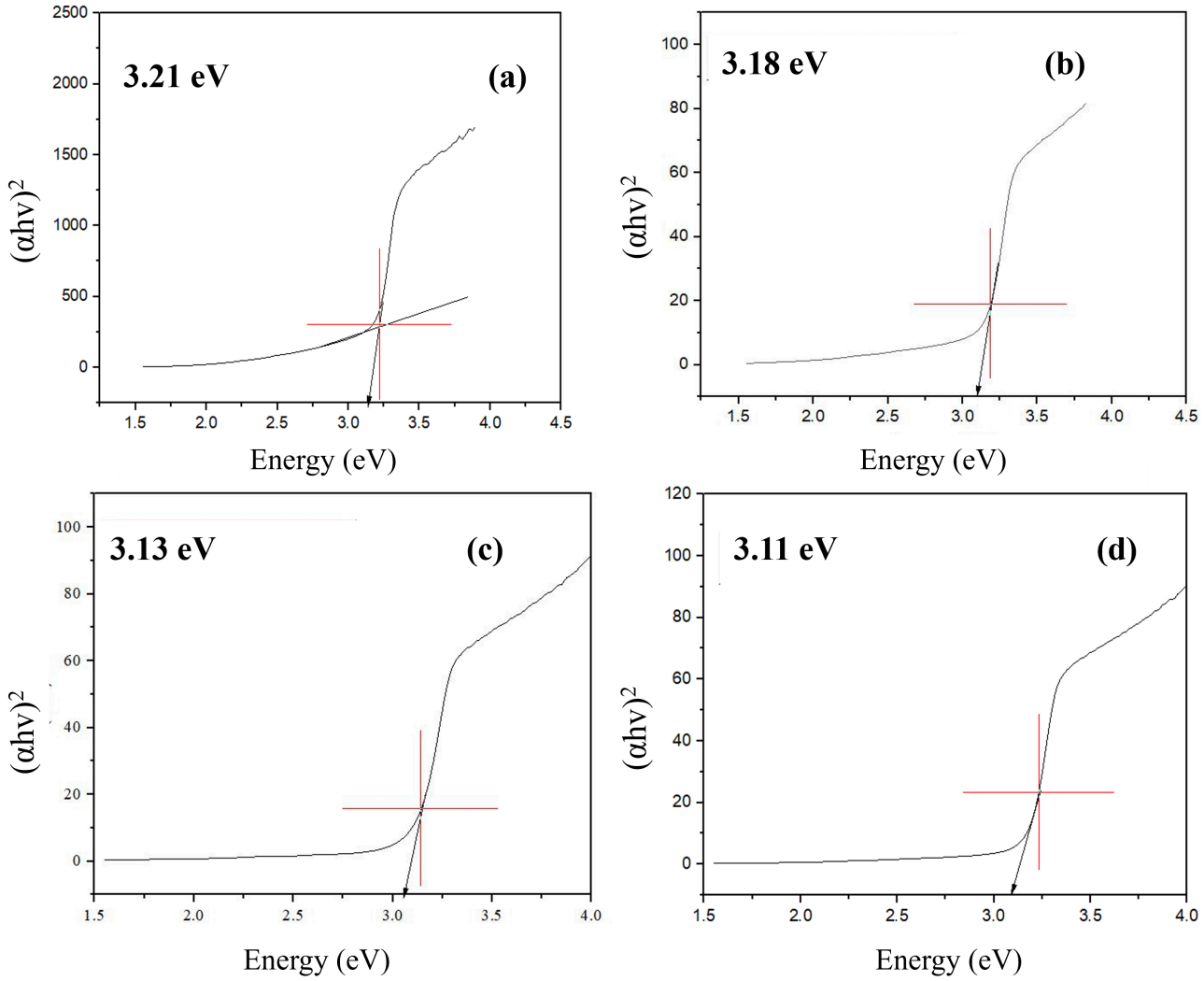

Figure 6. Tauc plots of (a) undoped ZnONPs, (b) 1% La-ZnONPs, (c) 2% La-ZnONPs, and (d) 3% La-ZnONPs. ZnONPs: zinc oxide nanoparticles; La-ZnONPs: lanthanum-doped ZnONPs.

Table 2. Average crystallite size and bandgap of undoped ZnONPs and La-ZnONPs on the basis of dopant concentration.

Products	Average crystallite size (nm)	Bandgap (eV)
ZnONPs	27.25	3.21
1% La-ZnONPs	25.68	3.18
2% La-ZnONPs	25.35	3.13
3% La-ZnONPs	21.27	3.11

ZnONPs: zinc oxide nanoparticles; La-ZnONPs: lanthanum-doped ZnONPs.

The observed reduction in crystallite size can be attributed to the emergence of La-O-Zn entities on the surfaces of the doped materials, which impede the process of crystallite growth, as elucidated by several researchers [6, 23, 24]. Similarly, this reduction may also stem from the dispersion of Zn-O-Zn matrix induced by La^{3+} ions, resultantly diminishes the accumulation rate of La-ZnONPs crystallization. However, XRD alone cannot conclusively confirm La^{3+} substitution into Zn^{2+} lattice sites because of the low dopant concentrations, but the observed variations are consistent with partial surface association, as supported by literature on similarly doped ZnO synthesis.

FTIR spectra of both undoped ZnONPs and La-ZnONPs (Figure 3b–e) preserve several functional groups originating from PPE, confirming surface adsorption at 3,360 cm^{-1}, 1,557 cm^{-1}, 1,403 cm^{-1}, indicated O–H stretching, C=O stretching of carbonyls, and COO bending vibrations, respectively. Upon La incorporation, new or intensified bands emerge at 782–855 cm^{-1}, assigned to Zn-O-La and La-O stretching, indicating lattice modification caused by La^{3+} substitution. The doped samples also retain weak O–H and

carbonyl bands, suggesting stronger binding of oxygenated organic residues due to increased surface coordination sites. The combined spectral evidence loss of extract peaks and emergence of Zn-O/La-O vibrations that confirms the effective role of plant biomolecules during green synthesis with embedding of La^{3+} into ZnO, and improved surface stabilization through residual organic ligands [25].

From 20,000× magnification of Figure 4, it can be seen that more pores exist and crystallization can obviously be seen. The discernible "pores" depicted in Figure 4b–d do not signify intrinsic porosity present within individual nanoparticles. On the contrary, these aspects are voids between particles formed by the aggregation process and the elimination of surplus organic compounds in the calcination method. Such voids are frequently observed in green-synthesized ZnO, attributable to phytochemical-mediated nucleation followed by subsequent thermal decomposition. These structural voids enhance the accessible surface area; however, they do not denote genuine microporosity at the level of individual nanoparticles.

The EDX spectra substantiate the presence of Zn and O as predominant elements across all samples, alongside detectable La signals in the doped specimens. The recorded atomic percentages depict the relative elemental composition. For instance, the La-doped sample containing 3% La exhibits a more substantial relative La signal in comparison to the samples containing 1% and 2% La, indicating an augmented incorporation of the dopant. From Figure 4a, the main constituents of the sample are Zn (78.97%) and O (21.03%). Figure 4d exhibits the highest elemental percentage of Zn (78.41%), while Figure 4c shows the highest elemental percentage of La (7.52%). We noticed that these materials preserved their nanoparticle structure even after calcination. Overall, the SEM-EDX results support the successful synthesis of ZnO nanoparticles modified with La dopant and demonstrate morphological changes that correlate with increased dopant concentration.

UV-Vis results reveal a slight red shift in the absorption edge and a reduction in bandgap energy from 3.21 to 3.11 eV. This difference in peak locations is likely caused by the photo-excitation of electrons from the valence band (VB) to the conduction band (CB). With the addition of La dopant, the absorption edge shows a small red shift and a marginal broadening toward longer wavelengths. Although the individual peak maxima in the spectra cannot be distinguished as separate values for each dopant concentration, the general pattern suggests that the optical response gradually changes as the La content increases. Such variations are frequently attributed to lattice strain, defect states, or localized energy levels introduced by rare-earth dopants, which can slightly decrease the effective bandgap and alter electron-hole dynamics. This steady bandgap narrowing is consistent with previous results on La-doped ZnO systems and can be attributed to the introduction of defect states and modifications to the electrical structure caused by La incorporation.

Tauc plots are derived from the data of UV-Vis spectra that give evidence of the bandgap decreasing trend, which is the effective point for any fabrication of photocatalyst. Tauc plots of undoped ZnONPs and 1%, 2%, and 3% La-ZnONPs are shown in Figure 6. According to the literature, ZnO exhibits bandgap energies ranging from 3.00 to 3.37 eV, depending on factors such as the synthesis method, morphology, and structure of the material [1, 26]. In this study, the findings indicated that the Eg energy for ZnONPs is lower than the values typically reported for bulk ZnONPs. Literature [19, 27, 28] shows that the value of Eg decreases due to the addition of dopants and increases the stability of nanoparticles.

This increase is attributed to suppression of crystallite growth, leading to smaller particle domains and more loosely packed aggregates, consistent with SEM and XRD observations. Thus, N_2 adsorption-desorption techniques were employed to examine further the BET-specific area and BJH pore size distribution of La-ZnONPs (Figure 7).

The nitrogen adsorption-desorption isotherms of undoped and La-ZnONPs exhibit type IV isotherms with H3-type hysteresis loops, confirming their mesoporous nature. The undoped ZnO shows the highest adsorption capacity, indicating a well-developed mesoporous network. Doping with 1% La reduces the adsorbed quantity and narrows the hysteresis loop, suggesting pore blocking. At 2% La, there is a significant decrease in adsorption volume and a broader hysteresis loop, indicating structural distortion. Increasing the La concentration to 3% partially restores the adsorption volume and leads to a more

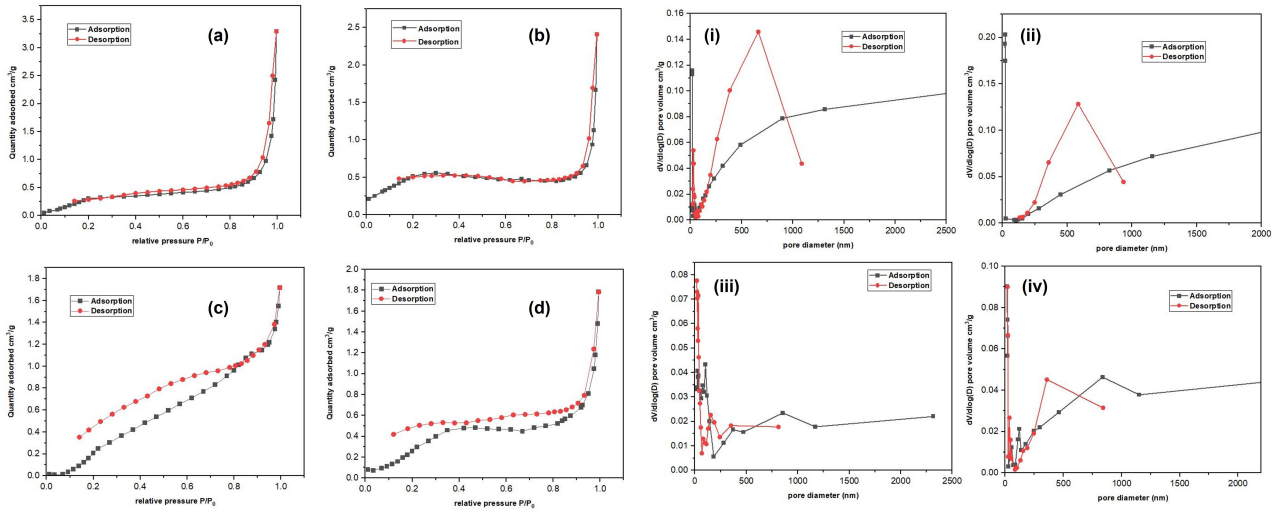

Figure 7. N_2 adsorption-desorption isotherms for fabricated (a) 1% La-ZnONPs, (b) 2% La-ZnONPs, (c) 3% La-ZnONPs, and (d) undoped ZnONPs, with insets of pore structure depicted as (i) 1% La-ZnONPs, (ii) 2% La-ZnONPs, (iii) 3% La-ZnONPs, and (iv) undoped ZnONPs. P/P_0 represents the relative pressure of nitrogen adsorption. La-ZnONPs: lanthanum-doped zinc oxide nanoparticles.

uniform pore-size distribution. Overall, La doping alters the textural properties of ZnO, diminishing mesoporosity at low to moderate levels before stabilizing at higher concentrations. The values of undoped and La-ZnONPs (1%, 2%, and 3%) specific surface area are mentioned in Table 3. As a photocatalytic activity, the surface area played a major role in enhancing the performance of the photocatalyst. By this analysis, it is clearly evident that more surface area provides more active sites for photocatalytic activity, and even the polyphenols from pineapple included in the fabrication of La-ZnONPs assisted in increasing this surface area as compared to previously studies fabricated La-ZnONPs [26, 29].

Table 3. Undoped and La-ZnONPs specific surface area and pore volume.

Sample	BET specific surface area (m^2/g)	Pore volume (cm^3/g)
Undoped ZnONPs	37.1206	0.0362
1% La-ZnONPs	38.8758	0.0464
2% La-ZnONPs	49.0049	0.0324
3% La-ZnONPs	65.4184	0.0493

La-ZnONPs: lanthanum-doped zinc oxide nanoparticles; BET: Brunauer-Emmett-Teller.

Formation chemistry behind La-ZnONPs synthesis in the presence of green source (pineapple extract)

In previous studies [5, 19, 30], there are many evidences on producing La-ZnONPs because La is considered a suitable candidate for doping and introduces new energy levels within the ZnONPs bandgap, reducing the energy required for photoactivation. But still, there is rare research done on using sustainable resources such as PPE or any biological source to increase the efficiency of fabricated photocatalysts.

The interactions between Zn^{2+} and La^{3+} ions during co-precipitation and calcination are due to phytochemicals presence in the extract. Pineapple peel is chosen as compared to other biological sources because there are no reported analysis-based results on the fabrication of La-ZnONPs assisted with PPE, and the polyphenols present in PPE enhance photoactivation effect by interacting with the doped material and also assist in reducing recombination rates, which prolongs the lifetime of photo-generated charge carriers, increasing photocatalytic efficiency [31, 32].

At the first stage, Zn^{2+} ions from zinc acetate and La^{3+} ions from La nitrate form coordination complexes with hydroxyl and carbonyl groups present in PPE, as depicted by the FTIR bands associated with O–H, C=O, and C–O vibrations. After the stage of NaOH addition dropwise to increase the pH to 11–12, these complexes undergo hydrolysis and lead to precipitation of $Zn(OH)_2$ and La-containing hydroxide

species. The presence of PPE-derived ligands around the forming hydroxide clusters modulates nucleation and growth, limiting uncontrolled aggregation.

At the drying and calcination at 300°C stage, the polyphenolic components from pineapple extract decompose while $Zn(OH)_2$ transforms into crystalline ZnO. The residual organic fragments on the nanoparticle surface are evidenced by the remaining O–H, C–H, and C=O bands in the FTIR spectra of ZnONPs and La-ZnONPs, indicating that a fraction of phytochemicals remains adsorbed as capping agents. These surface-bound groups contribute to the stabilization of nanoparticle aggregates and influence the formation of interparticle voids, consistent with the mesoporous-like features observed in the BET and SEM analyses.

La incorporation affects the formation chemistry by introducing larger La^{3+} ions into the system, which can induce lattice strain and modify the nucleation–growth balance. Overall, the combined FTIR, XRD, SEM-EDX, UV-Vis, and BET data support a green synthesis pathway in which PPE functions as both a complexing and capping agent, while La doping tunes the structural and surface properties of the resulting ZnO-based nanoparticles. Moreover, it is considered a sustainable approach in terms of green chemistry principles, waste valorization, and avoid usage of chemicals and tedious methods. To compare the present work with previous work that didn't utilize still green source, the data is given below in Table 4.

Table 4. La-ZnONPs from literature with specific data.

Fabricated nanoparticle	Method utilized	Green source	Bandgap (eV)	Surface area (m^2/g)	Reference
La-doped ZnO nanofibers	Electrospinning-calcination technology	Absent	3.1	11.15	[6]
La-doped ZnO granular nanocrystallites	Co-precipitation method	Absent	3.37	28.203	[33]
La-ZnONPs	Co-precipitation method	Absent	3.38	Not given	[30]
La-ZnONPs	Co-precipitation method	Pineapple extract	3.11	65.4184	Present work

La-ZnONPs: lanthanum-doped zinc oxide nanoparticles.

Hypothesized photocatalytic mechanism by La-ZnONPs based on the literature

It is important to point out that no photocatalytic degradation activity was conducted in this study. However, the observed features after analysis, such as decrease in bandgap energy, increase in specific surface area, and variation in morphology of La-ZnONPs synthesized in the presence of PPE, are considered favorable characteristics for photocatalytic applications. In this context, we provide here a brief literature-based mechanism as a hypothesis for how such green La-doped ZnO systems may operate under light irradiation, to guide future work.

When La-ZnONPs absorbed photons from visible light sources, the semiconductor's CB was activated by the electrons from the VB. Producing the electron-hole pairs (e^- and h^+) that are displayed in Equation 2.

$$La - ZnO + hv \rightarrow La - ZnO(e^- + h^+) \quad (2)$$

The photogenerated holes (h^+) can oxidize surface-adsorbed water or hydroxide ions to form hydroxyl radicals, while the electrons (e^-) reduce dissolved oxygen to superoxide radicals, shown in Equations 3 and 4.

$$h^+ + H_2O \rightarrow \cdot OH + H^+ \quad (3)$$

$$e^- + O_2 \rightarrow O_2.^- \quad (4)$$

Reactive oxygen species participate in the oxidation and degradation of organic pollutants (R), as commonly reported for ZnO-based photocatalysts, shown in Equation 5.

$$\cdot OH,\ O_2.^- + R \rightarrow intermediate \rightarrow CO_2\uparrow + H_2O + mineralized\ products \quad (5)$$

In the case of La-ZnONPs, La^{3+} acts as an electron trapper, resisting the recombination rate of e^- and h^+ and enhancing the life span of electrons and radicals. This eventually gives more time to electrons and holes to react with water and generate abundant free radicals ($O_2^{\cdot -}$ and $\cdot OH$), which subsequently degrade wastewater and different organic dyes. The mechanism of hypothesized photocatalytic activity of La-ZnONPs is illustrated in Figure 8.

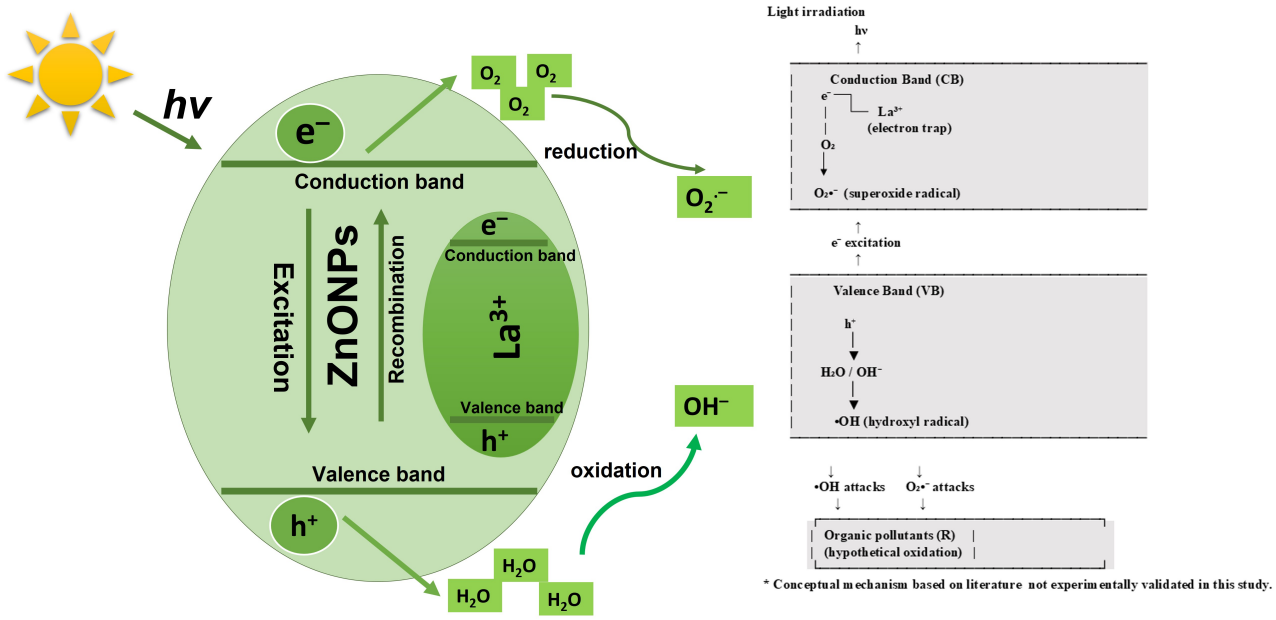

Figure 8. Literature-based hypothetical photocatalytic mechanism of La-ZnONPs. La denotes lanthanum dopant; hv represents photon energy. ZnONPs: zinc oxide nanoparticles; La-ZnONPs: La-doped ZnONPs.

This concept is consistent with the bandgap narrowing and increased surface area observed in this work, although it has not been experimentally verified here. The reaction scheme in Equations 1–4 should therefore be interpreted purely as a conceptual mechanism based on previously reported La-ZnO systems, serving as a starting point for future photocatalytic studies on the present materials.

Conclusion

ZnONPs and La-ZnONPs were successfully fabricated, assisted with a green and sustainable technique utilizing PPE as a natural source for reduction. Characterization through XRD, FTIR, SEM-EDX, UV-Vis, and BET analyses confirmed the synthesis. Structural characterization by XRD confirmed the formation of the hexagonal wurtzite ZnO phase for all samples, with La incorporation leading to a progressive decrease in crystallite size from 27.25 nm for undoped ZnONPs to 21.27 nm at 3% La. FTIR analysis revealed the presence of Zn-O vibrational modes alongside residual organic functional groups originating from PPE, indicating that phytochemicals participate in both nanoparticle formation and surface stabilization.

The results revealed that as the dopant concentration increased, both the crystallite size and bandgap of La-ZnONPs decreased. SEM-EDX observations showed aggregated nanoscale domains with morphological changes upon La addition, while EDX provided semi-quantitative evidence of La incorporation into the ZnO-based structures. UV-Vis results demonstrated a slight red shift in the absorption edge upon La doping, and Tauc analysis indicated that the optical bandgap decreased from approximately 3.21 eV (undoped) to 3.11 eV (3% La). BET surface area analysis further revealed that La doping substantially increased the specific surface area and pore volume, suggesting that dopant-induced modifications of crystallite size and aggregation behavior enhance accessible surface sites. Overall, this study demonstrates that integrating La doping with a PPE-assisted green synthesis route offers an environmentally friendly approach to tuning the structural and optical characteristics of ZnO-based nanomaterials.

Abbreviations

BET: Brunauer-Emmett-Teller

CB: conduction band

FTIR: fourier transform infrared spectroscopy

FWHM: full width at half maximum

$La(NO_3)_3 \cdot 6H_2O$: lanthanum nitrate hexahydrate

La: lanthanum

La-ZnONPs: lanthanum-doped zinc oxide nanoparticles

NaOH: sodium hydroxide

PPE: pineapple peel extract

SEM-EDX: scanning electron microscopy-energy dispersive X-ray

UV-Vis: ultra-violet visible

VB: valence band

XRD: X-ray diffraction

$Zn(CH_3COO)_2 \cdot 2H_2O$: zinc acetate dihydrate

ZnONPs: zinc oxide nanoparticles

Declarations

Acknowledgments

The authors sincerely express their acknowledgement to Universiti Malaysia Pahang Al-Sultan Abdullah, Lebuhraya Persiaran Tun Khalil Yaakob, 26300, Gambang, Kuantan Pahang, Malaysia for providing assistance during the completion of this study.

Author contributions

RTH: Conceptualization, Validation, Writing—original draft, Investigation, Visualization. NAP: Methodology, Data curation, Formal analysis. HA: Writing—review & editing. JHS: Supervision, Project administration, Funding acquisition. All authors read and approved the submitted version.

Conflicts of interest

The authors declare that they have no conflicts of interest.

Ethical approval

Not applicable.

Consent to participate

Not applicable.

Consent to publication

Not applicable.

Availability of data and materials

The raw data supporting the conclusions of this manuscript will be made available by the authors, without undue reservation, to any qualified researcher.

Funding

The authors are grateful to Universiti Malaysia Pahang Al-Sultan Abdullah for financial assistance for this project, grant no. RDU210134 (Ref. FRGS/1/ 2021/TK0/UMP/02/31). The funders had no role in study design, data collection and analysis, interpretation of results, writing of the manuscript, or the decision to submit the article for publication. Financial support was provided solely to cover laboratory analysis expenses.

Publisher's note

References

1. Patwa R, Rohilla S, saini J, Rani U. Characterization of structural and spectroscopic properties of ZnO/Fe_2O_3 nanocomposites. Ceram Int. 2024;50:47268–77. [DOI]
2. Raha S, Ahmaruzzaman M. ZnO nanostructured materials and their potential applications: progress, challenges and perspectives. Nanoscale Adv. 2022;4:1868–925. [DOI] [PubMed] [PMC]
3. Klinbumrung A, Panya R, Pung-Ngama A, Nasomjai P, Saowalakmeka J, Sirirak R. Green synthesis of ZnO nanoparticles by pineapple peel extract from various alkali sources. J Asian Ceram Soc. 2022;10: 755–65. [DOI]
4. Shukla M, Narain S, Kumar A, Dikshit A. Zinc oxide nanoparticles: A plant-mediated synthesis, characterizations and their functional applications. Nano Trends. 2026;13:100184. [DOI]
5. Tasaduq Hussain R, Afiqah S, Haslinda Shariffuddin J, Abdullah H. Green fabrication of Lanthanum doped Zinc Oxide Nanoparticles (La-ZnONPs) via Pineapple extract: Effects of Calcination Temperature on Photocatalytic Properties. In: Proceedings of 7th International Conference of Chemical Engineering & Industrial Biotechnology (ICCEIB 2024); 2024 Aug 27–29; Putrajaya, Malaysia. IOP Publishing; 2025. pp. 012016. [DOI]
6. Pascariu P, Homocianu M, Cojocaru C, Samoila P, Airinei A, Suchea M. Preparation of La doped ZnO ceramic nanostructures by electrospinning–calcination method: Effect of La^{3+} doping on optical and photocatalytic properties. Appl Surf Sci. 2019;476:16–27. [DOI]
7. Selvaraj S, Patrick DS, Manikandan VS, Vangari GA, Mohan MK, Navaneethan M. Synergistic effects of La-doping on ZnO nanostructured photocatalysts for enhanced MB dye degradation. Surf Interfaces. 2024;51:104538. [DOI]
8. Slimani Y, Khan A, Sivakumar R, Nawaz M, Thakur A. Synergistic impact of lanthanum and cerium co-doping ZnO for improved photocatalytic rhodamine B degradation efficiency under UV light. J Mol Struct. 2025;1322:140366. [DOI]
9. Hussain RT, Hossain MS, Shariffuddin JH. Green synthesis and photocatalytic insights: A review of zinc oxide nanoparticles in wastewater treatment. Mater Today Sustainability. 2024;26:100764. [DOI]
10. Shariffuddin JH, Ismail NAS, Razali NAM, Nayeem A. Phytochemical fabricated ZnO nanoparticles as photocatalyst using pineapple waste. In: Proceedings of 2ND PROCESS SYSTEMS ENGINEERING AND SAFETY (ProSES) SYMPOSIUM 2021; 2021 Dec 1; Pahang, Malaysia. AIP Publishing; 2023. pp. 040009. [DOI]
11. Zolfaghari M, Yadegar A, Rezaei A, Rafieian F, Kazemi M, Fazeli H, et al. Plant-mediated green synthesis of zinc oxide nanoparticles using *Anvillea garcinii* extract: Characterization and investigation of their anticancer, antibacterial and antioxidant effects. Ind Crops Prod. 2026;242:122785. [DOI]

12. Lopes IS, Oliveira de Moraes BN, de Souza Barreto S, Le Joncour L, Couteau C, Franzolin MR, et al. Green synthesis of antimicrobial silver–copper nanoparticles using Banana and pineapple peel extracts: A sustainable approach for biomaterial sterilization. Mater Chem Phys. 2025;333:130364. [DOI]
13. Eswaran P, Madasamy PD, Pillay K, Brink H. Sunlight-driven photocatalytic degradation of methylene blue using ZnO/biochar nanocomposite derived from banana peels. Biomass Conv Bioref. 2025;15: 12347–67. [DOI]
14. Mim MM, Saha P, Tonu NT, Akhe AS, Das T, Rahman SMM, et al. Eco-friendly synthesis of zinc oxide nanoparticles using *Citrus macroptera* peel extract and their role as a photocatalyst and antibacterial agent. Mater Today Commun. 2026;50:114452. [DOI]
15. Owoeye TF, Akinlabu DK, Ajayi OO, Afolalu SA, Popoola JO, Ajani OO. Phytochemical constituents and proximate analysis of dry pineapple peels. In: Proceedings of 5th International Conference on Science and Sustainable Development (ICSSD 2021); 2021 Oct 11–13; Nigeria. IOP Publishing; 2022. pp. 012027. [DOI]
16. Tran TV, Nguyen DTC, Nguyen TTT, Nguyen DH, Alhassan M, Jalil AA, et al. A critical review on pineapple (*Ananas comosus*) wastes for water treatment, challenges and future prospects towards circular economy. Sci Total Environ. 2023;856:158817. [DOI] [PubMed]
17. Sedefoglu N. Characterization and photocatalytic activity of ZnO nanoparticles by green synthesis method. Optik. 2023;288:171217. [DOI]
18. Alzura SP, Saraswaty V, Ishmayana S, Budiman YP, Eddy DR, Aji ES, et al. Synthesis and characterization of zinc oxide nanoparticles-carbon composite derived from pineapple peel wastes for adsorption of methylene blue from solution and photocatalytic activity. Case Stud Chem Environ Eng. 2025;11:101113. [DOI]
19. Iqbal T, Sohaib M. Synthesis of novel lanthanum-doped zinc oxide nanoparticles and their application for wastewater treatment. Appl Nanosci. 2021;11:2599–609. [DOI]
20. Soto B, Gatica M, Uribe EA, Rozas A, Cabezas R, Pino L, et al. Evaluation of antioxidant activity and polyphenol preservation in rosehip (Rosa spp.) during storage and convective drying. LWT. 2025;228: 118089. [DOI]
21. Antony A, Farid M. Effect of Temperatures on Polyphenols during Extraction. Appl Sci. 2022;12:2107. [DOI]
22. Suwanboon S, Amornpitoksuk P, Sukolrat A, Muensit N. Optical and photocatalytic properties of La-doped ZnO nanoparticles prepared via precipitation and mechanical milling method. Ceram Int. 2013; 39:2811–9. [DOI]
23. Shaban M, Zayed M, Hamdy H. Nanostructured ZnO thin films for self-cleaning applications. RSC Adv. 2017;7:617–31. [DOI]
24. Mao T, Liu M, Lin L, Cheng Y, Fang C. A Study on Doping and Compound of Zinc Oxide Photocatalysts. Polymers (Basel). 2022;14:4484. [DOI] [PubMed] [PMC]
25. Mirgane NA, Shivankar VS, Kotwal SB, Wadhawa GC, Sonawale MC. Waste pericarp of ananas comosus in green synthesis zinc oxide nanoparticles and their application in waste water treatment. Mater Today Proc. 2021;37:886–9. [DOI]
26. Lakshmi K, Mathusalini S, Arasakumar T, Kadirvelu K, Mohan PS. Highly reactive lanthanum doped zinc oxide nanofiber photocatalyst for effective decontamination of methyl parathion. J Mater Sci: Mater Electron. 2017;28:12944–55. [DOI]
27. Wu HH, Deng LX, Wang SR, Zhu BL, Huang WP, Wu SH, et al. The Preparation and Characterization of La Doped TiO_2 Nanotubes and Their Photocatalytic Activity. J Dispersion Sci Technol. 2010;31:1311–6. [DOI]
28. Rooshde MS, Abdullah WRW, Ibrahim NF, Ghazali MSM, Nik WMNW. Photocatalytic efficiency of lanthanide-doped zinc oxide for degradation of methylene blue dye. J Sustainability Sci Manage. 2018; 13:153–61.

29. Albiss B, Abu-Dalo M. Photocatalytic Degradation of Methylene Blue Using Zinc Oxide Nanorods Grown on Activated Carbon Fibers. Sustainability. 2021;13:4729. [DOI]
30. Kumar V, Sonia, Suman, Kumar S, Kumar D. Synthesis and characterization of lanthanum doped zinc oxide nanoparticles. In: Proceedings of International Conference on Condensed Matter and Applied Physics; 2015 Oct 30–31; Bikaner, India. AIP Publishing; 2016. pp. 020458. [DOI]
31. Poadang S, Yongvanich N, Phongtongpasuk S. Synthesis, Characterization, and Antibacterial Properties of Silver Nanoparticles Prepared from Aqueous Peel Extract of Pineapple, *Ananas comosus*. CMU J Nat Sci. 2017;16:123–33. [DOI]
32. Abd Hashib S, Ibrahim UK, Yahya A, Abd Rahman N. The Comparison of Bioactive Compounds and Antioxidant Activity of Fresh Pineapple and Pineapple Powder. J Adv Res Appl Sci Eng Technol. 2019; 17:54–60.
33. Jagtap RM, Kshirsagar DR, Khire VH, Pardeshi SK. Facile fabrication of porous La doped ZnO granular nanocrystallites and their catalytic evaluation towards thermal decomposition of ammonium perchlorate. J Solid State Chem. 2019;276:194–204. [DOI]